Original Article

DOI: 10.5582/ddt.2023.01035

# LncRNA SNHG1 upregulates FANCD2 and G6PD to suppress ferroptosis by sponging miR-199a-5p/3p in hepatocellular carcinoma

**Lin Zhou[1,§], Qing Zhang[1,2,§], Jiaxin Cheng[1], Xiandie Shen[1], Jing Li[1], Mingya Chen[1], Chang Zhou[1,*], Jianlin Zhou[1,*]**

[1] State Key Laboratory of Developmental Biology of Freshwater Fish & Key Laboratory of Protein Chemistry and Developmental Biology of the Ministry of Education, College of Life Science, Hunan Normal University, Changsha, Hunan, China;
[2] Clinical Research Center for Reproduction and Genetics in Hunan Province, Reproductive and Genetic Hospital of CITIC-Xiangya, Changsha, Hunan, China.

**SUMMARY** Ferroptosis is a form of regulated cell death (RCD) triggered by iron-dependent lipid peroxidation and is closely associated with the occurrence and progression of hepatocellular carcinoma (HCC). The lncRNA SNHG1 (small nucleolar RNA host gene 1) has been shown to play an oncogenic role in HCC, but its function in RCD other than autophagy and apoptosis is still unknown. Here, we investigated the correlation between SNHG1 and 156 typical markers of five RCD types based on RNA sequencing data from The Cancer Genome Atlas database and showed the negative regulators of ferroptosis FANCD2 (Fanconi anemia complementation group D2) and G6PD (glucose-6-phosphate dehydrogenase) to be the most highly and fifth most highly correlating factors with SNHG1, respectively. A competitive endogenous RNA network of SNHG1 – miR-199a-5p/3p – FANCD2/G6PD was constructed bioinformatically. *In vitro* experiments showed that overexpression of the miR-199a precursor led to a decrease in expression of SNHG1, FANCD2, and G6PD, whereas knockdown of SNHG1 decreased expression of FANCD2 and G6PD but increased levels of miR-199a-5p and miR-199a-3p in HCC cells (Huh7 and HepG2). In addition, knockdown of SNHG1 increased erastin-mediated ferroptosis, iron accumulation, and lipid peroxidation. These results suggest that SNHG1 upregulates FANCD2 and G6PD by sponging miR-199a, thereby inhibiting ferroptosis in HCC. Moreover, a signature based on expression of SNHG1, FANCD2, and G6PD was identified as being associated with overall survival and the immunological microenvironment in HCC. Collectively, this study identified the SNHG1–miR-199a–FANCD2/G6PD axis in HCC, which is a potential marker for the prognosis and therapy of this tumor.

***Keywords*** ferroptosis, FANCD2, G6PD, SNHG1, hepatocellular carcinoma

## 1. Introduction

Liver cancer is one of the most common and lethal types of cancers. According to global cancer statistics, the incidence and mortality of primary liver cancer ranked sixth and third, respectively, in 2020 (*1*). Hepatocellular carcinoma (HCC) and intrahepatic cholangiocarcinoma are the two major types of primary liver cancers, accounting for 75-85% and 10-15% of cases, respectively (*1*). Due to limited detection capabilities and the asymptomatic nature of HCC in early stages, most patients are diagnosed at a late stage and thus miss the chance of radical resection (*2*). The 5-year overall survival (OS) rate of HCC patients is only 19.5% (*3*). Hence, there is an urgent need to elucidate the molecular pathogenesis of HCC to improve the efficacy of diagnosis and treatment.

Recently, regulated cell death (RCD) has gained increasing attention from cancer researchers. RCD, also called programmed cell death, refers to a type of cell death that is regulated by genes and differs from uncontrolled and random cell death (*4,5*). The major types of RCD include apoptosis, autophagy, pyroptosis, necroptosis, PANoptosis, ferroptosis, and the newly discovered cuproptosis (*6*). Ferroptosis, a form of RCD induced by iron-dependent lipid peroxidation, was first discovered by Dixon *et al*. (*7*). Ferroptosis has been shown to be highly related to the occurrence and

progression of HCC and can be used as a therapeutic target and prognostic factor (*8, 9*).

The lncRNA SNHG1 plays an important role in various cancers, including HCC (*10*). Our previous study showed that SNHG1 (small nucleolar RNA host gene 1) acts as a competitive endogenous RNA (ceRNA) to regulate the cell cycle in HCC (*11*). However, its role in RCDs other than apoptosis and autophagy has not been investigated. In the present study, we performed coexpression analysis of SNHG1 and 156 RCD-related genes based on RNA sequencing (RNA-seq) data. According to the Pearson correlation coefficient, the ferroptosis-related genes *FANCD2* (Fanconi anemia complementation group D2) and *G6PD* (glucose-6-phosphate dehydrogenase) are the most highly and fifth most highly correlating factors with SNHG1, respectively. Therefore, we investigated the role and molecular mechanism of SNHG1 in ferroptosis and constructed a prognostic signature for predicting OS and response to immunotherapy in patients with HCC.

## 2. Materials and Methods

### 2.1. RNA-seq data acquisition

RNA-seq data and clinical information of patients with HCC were obtained from The Cancer Genome Atlas (TCGA) and International Cancer Genome Consortium (ICGC) databases. The TCGA cohort included 374 HCC tissues and 50 adjacent normal liver tissues. The ICGC cohort (LIRI-JP) included 243 HCC tissue samples and 202 adjacent nontumor liver tissue samples. In addition, microRNA (miRNA) expression RNA-seq data (371 HCC tissues and 49 adjacent normal liver tissues) were obtained from the TCGA database.

### 2.2. Cell lines, chemicals, and antibodies

The HCC cell lines HepG2 and Huh7 were obtained from American Type Culture Collection (ATCC) (Manassas, VA, USA) and cultured according to ATCC's instructions. All cell lines were free of mycoplasma and authenticated by Yubo Biological Technology (Shanghai, China) using short tandem repeat analysis. Erastin and FeRhoNox-1 ($Fe^{2+}$ indicator) were purchased from Selleck (Houston, TX, USA) and MKBio (Shanghai, China), respectively. The antibodies used in this study were purchased from ABclonal (Wuhan, Hubei, China). MTT [3-(4,5-dimethylthiazol-2-yl)-2,5 diphenyl tetrazolium bromide] was purchased from Beyotime (Shanghai, China).

### 2.3. Lentivirus infection

Lentiviruses expressing SNHG1 shRNA or the microRNA-199a (miR-199a) precursor (hsa-mir-199a-1) were purchased from GeneChem (Shanghai, China). The target sequence of the SNHG1 shRNA was validated in our previous study (*11*). Lentivirus particles were transduced into cells according to the manufacturer's instructions. At 72 hours after transduction, the cells were cultured in fresh medium with hygromycin B to generate stable cell lines.

### 2.4. Western blotting

As previously described (*11*), total cellular proteins were extracted, separated, and transferred to a polyvinylidene fluoride (PVDF) membrane. After blocking, the membranes were cut into pieces and incubated separately with antibodies. Protein bands were visualized using the ChemiLucent ECL Detection System (Millipore, Billerica, MA, USA).

### 2.5. RNA isolation and reverse-transcription quantitative PCR (RT-qPCR)

Total RNA was isolated from cell lines using TRIzol reagent (Invitrogen, Carlsbad, CA, USA) and served as a template for the RT reaction. mRNAs were reverse-transcribed into cDNA using a First-Strand cDNA Synthesis Kit (GeneCopoeia, Guangzhou, Guangdong, China). Primers for 18S rRNA and SNHG1 have been described previously (*11*). The primers used for FANCD2 and G6P were as follows: FANCD2, 5′-ACATACCTCGACTCATTGTCAGT-3′ (forward) and 5′- TCGGAGGCTTGAAAGGACATC-3′ (reverse); G6PD, 5′- CGAGGCCGTCACCAAGAAC-3′ (forward) and 5′- GTAGTGGTCGATGCGGTAGA-3′ (reverse). For miRNA RT, miRNA was first polyA-tailed and reverse-transcribed using oligo-dT primers provided in miRNA First-Strand cDNA Synthesis Kit (GeneCopoeia). SYBR Green-based real-time PCR was performed using a qPCR kit (GeneCopoeia).

### 2.6. Analysis of erastin-mediated ferroptosis

Cells were plated in 96-well plates and treated with various concentrations of erastin for 48 h. Cell viability was determined by MTT assays as described previously (*11*).

### 2.7. Analysis of iron accumulation

Cells were seeded onto glass coverslips. After aspiration of the culture medium, the cells were washed twice with phosphate-buffered saline (PBS) and stained with FeRhoNox-1 (5 μmol/L) for 60 min at 37°C in a 5% $CO_2$ incubator. The cells were then observed under a fluorescence microscope.

### 2.8. Malondialdehyde (MDA) assay

Cells were incubated with thiobarbituric acid (TBA) at

95°C for 60 min and cooled in an ice bath for 10 min. The MDA concentration was quantified calorimetrically (OD = 532 nm).

2.9. Identification of SNHG1-associated typical RCD markers

Pearson correlation analysis was performed to investigate the coexpression relationship between SNHG1 and 156 typical markers of RCD from previous studies (*6,12*).

2.10. Construction of the ceRNA network

The ceRNA network was constructed as previously described (*11*). Differential expression of RNAs between HCC tissue and adjacent normal liver tissue was identified using the 'limma' package of R software (*https://www.r-project.org/*). StarBase (*https://starbase.sysu.edu.cn/index.php*) and the miRWalk database (*http://mirwalk.umm.uni-heidelberg.de/*) were used to predict potential lncRNA–miRNA and miRNA–mRNA pairs, respectively. The ceRNA network was visualized using the R package "ggalluvial."

2.11. Construction and validation of a prognostic signature

The TCGA cohort was used to construct a prognostic model, and the ICGC cohort was used to validate this model. Univariate and multivariate Cox regression analyses were performed to examine the correlation between gene expression with the R package "survival". The risk score for each patient was then calculated based on the coefficient of multivariate Cox regression analysis. A Kaplan–Meier (KM) survival curve was used to calculate survival difference between the high- and low-risk groups using the R packages "survival" and "survminer". Multivariate Cox regression analysis was performed to evaluate whether the risk score is an independent prognostic predictor of OS when other clinical factors (age, sex, stage, grade, T stage, N stage, and M stage) are considered. A receiver operating characteristic (ROC) curve was produced using the R package "timeROC" to evaluate the predictive power of the signature.

2.12. Comparison of immunity status between high- and low-risk groups

To evaluate the role of the risk model in the immunological microenvironment, we compared the proportions of 22 different immune cell types between patients with high- or low-risk score using CIBERSORT. CIBERSORT is an algorithm that uses a set of reference gene expression matrices to evaluate the proportions of immune cell types from bulk tumor sample expression data based on the principle of linear support vector regression (*13*). In addition, we compared differential expression of immune checkpoint genes between the high- and low-risk groups. Response to immune checkpoint inhibitor (ICI) immunotherapy in HCC patients was predicted using Tumor Immune Dysfunction and Exclusion (TIDE) (*http://tide.dfci.harvard.edu*) (*14*) and IMvigor210 (*15*) algorithms.

2.13. Statistical analysis

All statistical analyses were performed using R language. One-way analysis of variance (ANOVA) was used to assess differences between groups. Pearson's correlation test was used for correlation analysis. The log-rank test was used to evaluate the significance of differences in survival curves. Statistical significance was set at $p < 0.05$.

**3. Results**

3.1. SNHG1 correlates positively with the ferroptosis-related genes *FANCD2* and *G6PD*

We analyzed the coexpression relationship between SNHG1 and RCD markers based on RNA-seq data from TCGA (including 374 HCC tissue and 50 adjacent normal liver tissue specimens). According to previous literature (*6,12*), 156 typical markers of five RCD types, including ferroptosis, pyroptosis, necroptosis, PANoptosis, and cuproptosis, were selected for coexpression analysis. The negative regulators of ferroptosis FANCD2 and G6PD were found to correlate highly with SNHG1, with the first and fifth highest correlation coefficients (cor): cor (FANCD2, SNHG1) = 0.76, cor (G6PD, SNHG1) = 0.63 (Figure 1A). Similar to SNHG1(11), FANCD2 and G6PD were significantly overexpressed in HCC tissues (Figure 1B). These results suggest that SNHG1 is involved in ferroptosis.

3.2. Bioinformatic identification of a ceRNA network of SNHG1–miRNAs–FANCD2/G6PD

The above results showed that SNHG1 is coexpressed with FANCD2 and G6PD. According to the ceRNA hypothesis (*16*), SNHG1 is a potential ceRNA of FANCD2 and G6PD. Therefore, we constructed a ceRNA network of lncRNAs, miRNAs, and mRNAs. miRNAs targeting lncRNA SNHG1 and mRNA (FANCD2 and G6PD) were predicted using starBase and miRWalk software, respectively. A total of 87 common miRNAs targeting both lncRNA SNHG1 and mRNA (FANCD2 or G6PD) were identified (Figure 1C). In the ceRNA network, miRNAs correlate negatively with lncRNAs and mRNAs (*16*). Considering the lncRNA SNHG1 and mRNAs (FANCD2 or G6PD) to be overexpressed in HCC, we selected common miRNAs targeting both SNHG1 and FANCD2 (or G6PD) from

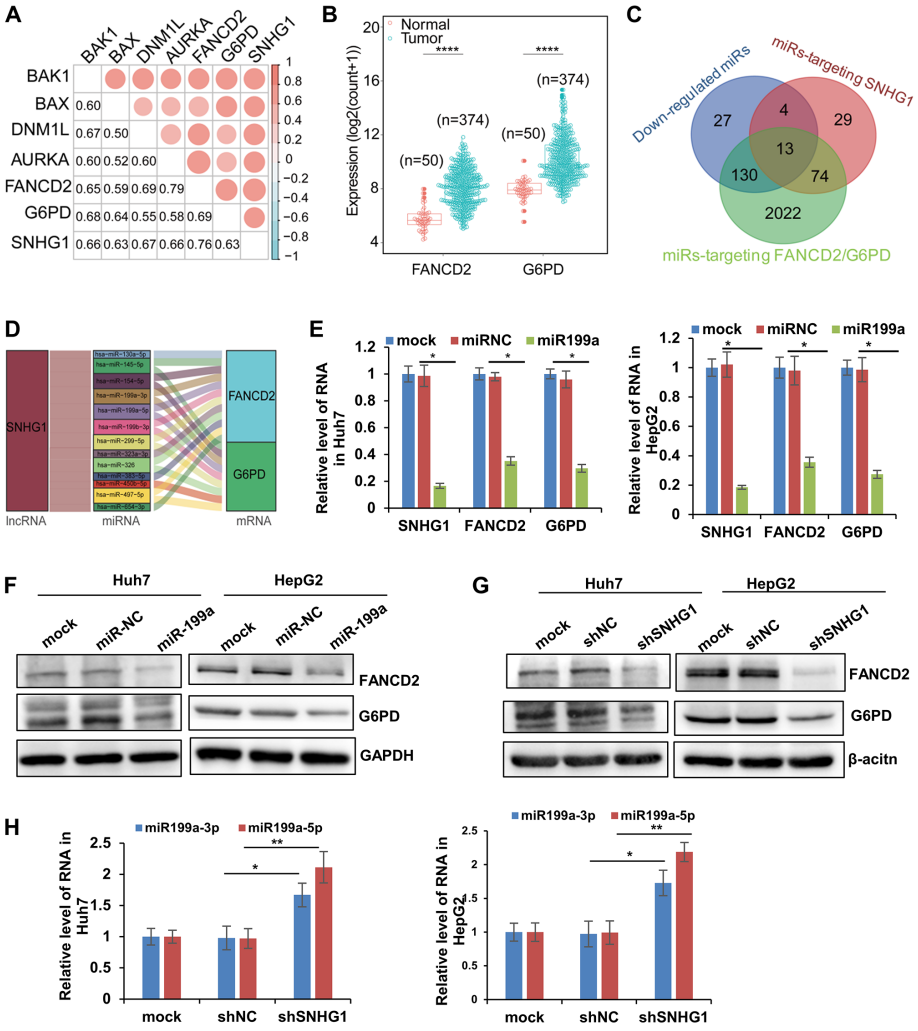


**Figure 1. SNHG1 upregulates FANCD2 and G6PD as a ceRNA.** (**A**) The coexpression relationship between SNHG1 and RCD markers was determined based on RNA-seq data from TCGA, and the top 7 genes with the highest coefficient are shown. (**B**) Differential expression of FANCD2 and G6PD between HCC and noncancerous liver tissues in TCGA cohorts. (**C**) Venn diagram showing the number of predicted miRNAs targeting FANCD2, G6PD and SNHG1 and downregulated miRNAs. (**D**) A ceRNA network of SNHG1–miRNAs–FACD2/G6PD. (**E-F**) The effect of miR-199a on expression of SNHG1, FANCD2, and G6PD. At 72 hours after infection with lentivirus particles expressing scrambled miRNA (miRNC) or premiR-199a (miR199a), the RNA and protein levels of SNHG1, FANCD2, and G6PD were detected by RT-qPCR (**E**) and western blotting (**F**), respectively. (**G-H**) The effect of SNHG1 on expression of FANCD2, G6PD and miR-199a-5p/3p. At 72 hours after infection with lentivirus particles expressing empty vector (shNC) or SNHG1 (shSNHG1), levels of FANCD2 and G6PD proteins and levels of miR-199a-5p and miR-199a-3p were detected by western blotting (**G**) and RT-qPCR (**H**), respectively. *$p < 0.05$, **$p < 0.01$.

the downregulated miRNAs (Figure 1C). As a result, 13 downregulated miRNAs met the criteria and were used to construct the ceRNA network (Figure 1D). These results suggest that SNHG1 regulates FANCD2 and G6PD by sponging 13 miRNAs.

### 3.3. Experimental validation of the SNHG1–miR-199a–FANCD2/G6PD axis

Interestingly, SNHG1, FANCD2, and G6PD were the common targets of miR-199a-5p and miR-199a-3p, which derive from the 5' and 3' arms of the same miRNA precursor, premiR-199a. Therefore, we transduced lentivirus particles expressing premiR-199a into HepG2 and Huh7 cells. The results of qPCR and western blotting analyses showed that overexpression of premiR-199a resulted in a decrease in expression of SNHG1, FANCD2, and G6PD (Figures 1E and 1F). This suggests that SNHG1, FANCD2, and G6PD are targets of miR-199a. Moreover, knockdown of SNHG1 decreased expression of FANCD2 and G6PD (Figure 1G) but increased levels of miR-199a-5p and miR-199a-3p (Figure 1H). These results indicate that SNHG1 increases expression of FANCD2 and G6PD by sponging miR-199a-5p/3p.

### 3.4. Suppression of SNHG1 promotes ferroptosis

The above results show that SNHG1 upregulates expression of FANCD2 and G6PD by sponging miR-199a-5p/3p, but FANCD2 and G6PD suppress ferroptosis (*17,18*). Therefore, we investigated whether

SNHG1 inhibits erastin-induced ferroptosis. As expected, SNHG1 knockdown increased erastin-mediated cytotoxicity in both Huh7 and HepG2 cells (Figures 2A and 2B), suggesting that SNHG1 protects HCC cells from ferroptosis. Ferroptosis is characterized by iron accumulation and lipid peroxidation (*19*). The effect of SNHG1 on iron accumulation and lipid peroxidation was determined using an $Fe^{2+}$ indicator and MDA assay, respectively. The product of lipid peroxidation (Figures 2C and 2D) and the $Fe^{2+}$ concentration (Figures 2E and 2F) increased in SNHG1-deficient cells with or without erastin treatment, suggesting that SNHG1 decreases iron accumulation and lipid peroxidation.

### 3.5. The prognostic value of a signature based on expression of SNHG1, FANCD2 and G6PD

Our previous study showed SNHG1 expression to act as a prognostic factor for OS in patients with HCC (*11*). Univariate and multivariate Cox regression analyses were performed to assess correlations between gene expression and OS. Based on univariate Cox regression analysis, both FANCD2 and G6PD are risk factors for HCC, similar to SNHG1 (Figure 3A). A three-gene signature was generated based on the multivariate Cox regression coefficient (Figure 3B), and the risk score of each patient was calculated using the following formula: risk score = 0.29873 × G6PD + 0.01513 × SNHG1 + 0.05200 × FANCD2.

To assess the prognostic significance of the risk model, we investigated the correlation between the risk score and clinical parameters. The patients in the TCGA and ICGC cohorts were divided into high- and low-risk groups according to the median risk score (cutoff value: 3.516333 in TCGA and 6.192844 in ICGC). Kaplan–Meier analysis showed that patients in the high-risk group had significantly worse survival than patients in the low-risk group in the TCGA (Figure 3C) and ICGC cohorts (Figure 3D). Moreover, time-dependent ROC analyses showed that this signature has high predictive ability. The area under the curve (AUC) of 1-year, 3-year, and 5-year survival in TCGA was 0.765, 0.666, and 0.633 (TCGA), respectively (Figure 3E). The AUCs of 1-year, 2-year, and 3-year survival in the ICGC cohort were 0.657, 0.706, and 0.765, respectively (Figure 3F). Multivariate Cox regression analysis showed that the risk

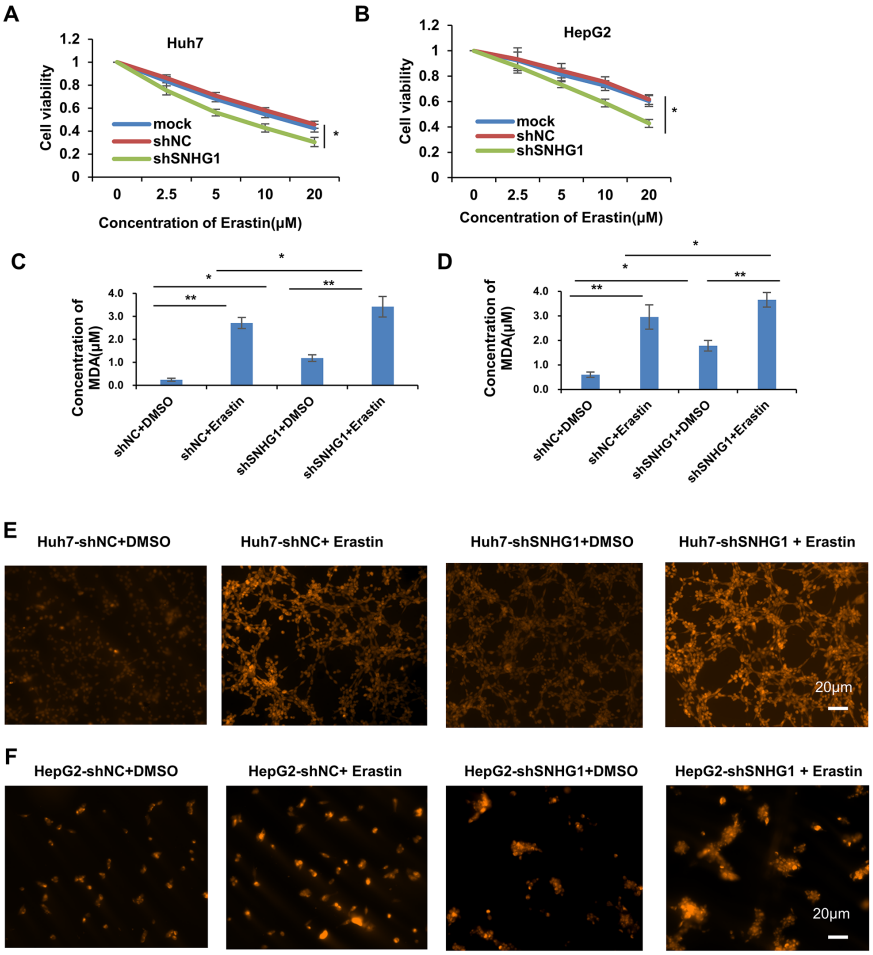


**Figure 2. Suppression of SNHG1 promotes ferroptosis.** Cells stably expressing empty vector (shNC) or SNHG1 (shSNHG1) were treated with different concentrations of erastin for 48 hours. (**A-B**) Cell viability was determined by MTT assays. (**C-D**) The MDA concentration was quantified by calorimetry. (**E-F**) The intracellular iron concentration was detected by the $Fe^{2+}$ indicator FeRhoNox-1. *$p < 0.05$, **$p < 0.01$.

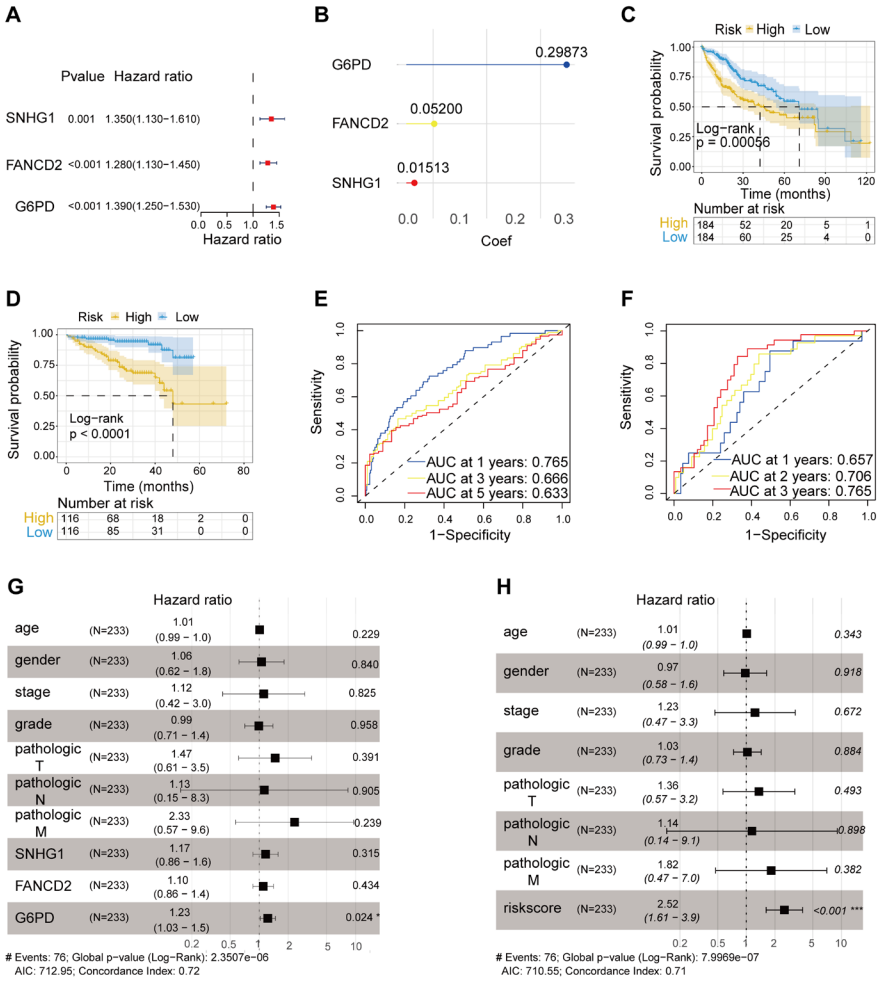


**Figure 3. Construction and validation of a prognostic signature based on expression of SNHG1, FANCD2, and G6PD.** (**A-B**) Univariate (**A**) and multivariate Cox regression (**B**) analyses were performed to assess the correlation between gene expression and overall survival. (**C-D**) Kaplan–Meier survival curves for low- and high-risk groups in TCGA (**C**) and ICGC cohorts (**D**). (**E-F**) Time-dependent ROC curve analyses of prediction models for survival in TCGA (**E**) and ICGC cohorts (**F**). **(G-H)** Multivariate analyses of factors associated with overall survival.

score and G6PD can serve as independent prognostic factors for patients with HCC when other clinical factors (age, sex, stage, grade, T stage, N stage, and M stage) are considered (Figures 3G-3H).

### 3.6. The value of the signature in predicting response to immunotherapy

To evaluate the role of the risk model in the immune microenvironment of HCC, the CIBERSORT algorithm was used to compare the 22 different immune cell types in HCC to evaluate the role of the risk model in the immune microenvironment of HCC. We found that 10 of these immune cell types were differentially expressed between the two risk groups. In patients with high risk scores, M2 macrophages, resting CD4 T cells, and resting mast cells were downregulated, whereas resting dendritic cells, M0 macrophages, activated CD4 T cells, and Treg cells were upregulated (Figure 4A). In addition, we determined whether there is a correlation between expression of inhibitory immune checkpoints and the risk score. Interestingly, expression levels of almost all checkpoints were significantly upregulated in the high-risk group (Figure 4B). Moreover, the high-risk group had a higher TIDE score than the low-risk group (Figure 4C). These results suggest that the risk score is associated with immune suppression. However, according to IMvigor210 analysis, the high-risk group had higher rates of complete response (CR) and partial response (PR) to ICI immunotherapy than the low-risk group (Figure 4D). This suggests that patients with high risk scores benefit more from ICI treatment.

## 4. Discussion

In the present study, we investigated the correlation between SNHG1 and typical markers of five RCD (ferroptosis, pyroptosis, necroptosis, PANoptosis, and cuproptosis). We found that SNHG1 correlated most strongly with the ferroptosis markers FANCD2 and G6PD. SNHG1 normally functions as a ceRNA for miRNAs in cancer (*10,11*). In the present study, a ceRNA network of SNHG1–miRNAs–FANCD2/G6PD was bioinformatically constructed, and the regulatory axis of

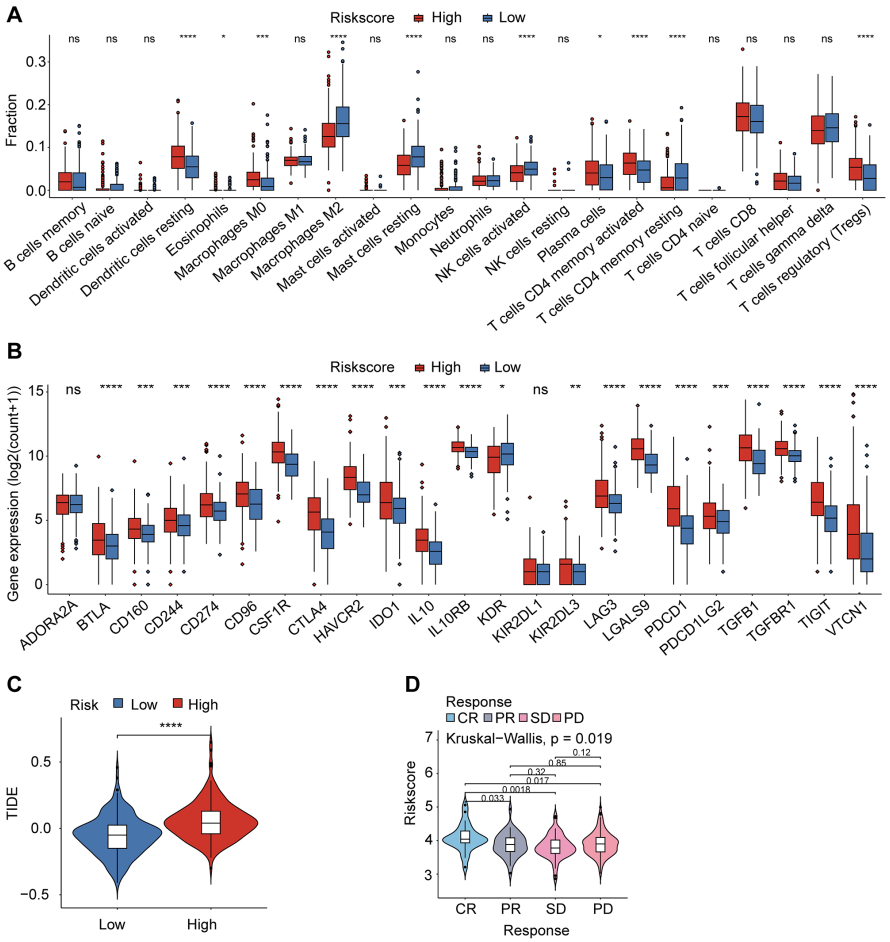


**Figure 4. The gene signature based on expression of SNHG1, FANCD2, and G6PD is associated with the immune microenvironment.** (**A**) The difference in the degree of immune infiltration of 22 immune cell types between the high- and low-risk groups, as assessed by the CIBERSORT algorithm. (**B**) The difference in expression of immune checkpoints between high- and low-risk groups. (**C-D**) Response to immunotherapy in HCC patients was estimated using TIDE (**C**) and IMvigor210 (**D**) algorithms. *$p < 0.05$, **$p < 0.01$, ***$p < 0.001$, ****$p < 0.0001$.

SNHG1–miR-199a–FANCD2/G6PD was experimentally validated. FANCD2 and G6PD are negative regulators of ferroptosis. FANCD2 inhibits ferroptosis by suppressing iron accumulation and lipid peroxidation (*17*). The repressive role of G6PD in ferroptosis is associated with the P450 metabolic pathway (*18*). We demonstrated that knockdown of SNHG1 or overexpression of premiR-199a decreased expression of FANCD2 and G6PD and that knockdown of SNHG1 enhanced erastin-induced ferroptosis in HCC cells. These results indicate that SNHG1 upregulates FANCD2 and G6PD by sponging miR-199a-5p/3p, thereby inhibiting ferroptosis. To our knowledge, this is the first report on involvement of SNHG1 in ferroptosis.

According to the miRBase database (*https://www.mirbase.org*), there are two miR-199a precursors: premir-199a-1 on chromosome 19 and premir-199a-2 on chromosome 1. Both precursors can be processed into mature miR-199a-5p and miR-199a-3p. Both miR-199a-5p and miR-199a-3p are known tumor suppressors in HCC (*20-22*). They regulate several cellular processes in cancer, including proliferation, apoptosis, migration, and invasion (*20-22*). Only two groups have reported the effects of miR-199a on ferroptosis; however, the results are conflicting. Lin *et al.* (*23*) reported that miR-199a-3p suppresses endothelial cell ferroptosis by targeting SP1. However, according to a study by Zhang *et al.*, miR-199a-5p stimulates ferroptosis-induced death of cardiomyocytes during ischemic/hypoxic injury by inhibiting the Akt/eNOS signaling pathway (*24*). It is possible that miR-199a exerts different effects by targeting different targets. However, it is unknown whether miR-199a regulates ferroptosis in cancer cells. Here, we report that overexpression of premiR-199a decreases expression of the negative regulators of ferroptosis FANCD2 and G6PD. This suggests that miR-199a exerts its antitumor activity by promoting ferroptosis.

Ferroptosis is a type of cell death induced by iron-dependent lipid peroxidation (*19*), and hepatocytes are the main cells involved in iron storage (*25*). Accumulating evidence has demonstrated that HCC cells can inactivate ferroptosis through multiple mechanisms and that activating ferroptosis is a

potential strategy for HCC cancer treatment (*26*). In addition, activation of ferroptosis can regulate the tumor immune microenvironment and sensitize cancer cells to immunotherapy (*27*). In the present study, we demonstrated that SNHG1, FANCD2 and G6PD are inhibitors of ferroptosis and constructed a signature based on SNHG1, FANCD2 and G6PD expression. The risk score calculated using this signature was an independent prognostic factor for OS in patients with HCC. Moreover, this risk score was associated with infiltration of immune cells and expression of immune checkpoints.

In conclusion, the present study demonstrates that SNHG1 upregulates FANCD2 and G6PD by sponging miR-199a-5p and miR-199a-3p, thereby inhibiting ferroptosis in HCC. Furthermore, a signature based on expression of SNHG1, FANCD2, and G6PD was identified as an independent prognostic marker for OS and associated with the proportion of infiltrating immune cell types, immune checkpoint expression, and response to immunotherapy. These findings are useful to further elucidate the pathogenesis of HCC and develop new strategies for clinical treatment and diagnosis.

**Acknowledgements**

The results published here are in part based upon data from The Cancer Genome Atlas (*https://portal.gdc.cancer.gov/*) and International Cancer Genome Consortium (*https://dcc.icgc.org*).

*Funding*: This work was supported by the National Natural Science Foundation of China (grant No. 82070155) and the Natural Science Foundation of Changsha (grant No. kq2202249).

*Conflict of Interest*: The authors have no conflicts of interest to disclose.

**References**

1. Sung H, Ferlay J, Siegel RL, Laversanne M, Soerjomataram I, Jemal A, Bray F. Global cancer statistics 2020: GLOBOCAN estimates of incidence and mortality worldwide for 36 cancers in 185 countries. CA Cancer J Clin. 2021; 71:209-249.
2. Rattanasupar A, Chartleeraha S, Akarapatima K, Chang A. Factors that affect the surveillance and late-stage detection of a newly diagnosed hepatocellular carcinoma. Asian Pac J Cancer Prev. 2021; 22:3293-3298.
3. Wang CY, Li S. Clinical characteristics and prognosis of 2887 patients with hepatocellular carcinoma: A single center 14 years experience from China. Medicine (Baltimore). 2019; 98:e14070.
4. Tang D, Kang R, Berghe TV, Vandenabeele P, Kroemer G. The molecular machinery of regulated cell death. Cell Research. 2019; 29:347-364.
5. Peng F, Liao M, Qin R, Zhu S, Peng C, Fu L, Chen Y, Han B. Regulated cell death (RCD) in cancer: Key pathways and targeted therapies. Signal Transduct Target Ther. 2022; 7:286.
6. Tsvetkov P, Coy S, Petrova B, *et al*. Copper induces cell death by targeting lipoylated TCA cycle proteins. Science. 2022; 375:1254-1261.
7. Dixon SJ, Lemberg KM, Lamprecht MR, Skouta R, Zaitsev EM, Gleason CE, Patel DN, Bauer AJ, Cantley AM, Yang WS, Morrison B 3rd, Stockwell BR. Ferroptosis: An iron-dependent form of nonapoptotic cell death. Cell. 2012; 149:1060-1072.
8. Wang W, Pan F, Lin X, Yuan J, Tao C, Wang R. Ferroptosis-related hub genes in hepatocellular carcinoma: Prognostic signature, immune-related, and drug resistance analysis. Front Genet. 2022; 13:907331.
9. Zhang B, Bao W, Zhang S, Chen B, Zhou X, Zhao J, Shi Z, Zhang T, Chen Z, Wang L, Zheng X, Chen G, Wang Y. LncRNA HEPFAL accelerates ferroptosis in hepatocellular carcinoma by regulating SLC7A11 ubiquitination. Cell Death Dis. 2022; 13:734.
10. Thin KZ, Tu JC, Raveendran S. Long non-coding SNHG1 in cancer. Clin Chim Acta. 2019; 494:38-47.
11. Zhou L, Zhang Q, Deng H, Ou S, Liang T, Zhou J. The SNHG1-centered ceRNA network regulates cell cycle and is a potential prognostic biomarker for hepatocellular carcinoma. Tohoku J Exp Med. 2022; 258:265-276.
12. Gong L, Huang D, Shi Y, Liang Z, Bu H. Regulated cell death in cancer: From pathogenesis to treatment. Chin Med J (Engl). 2023; 136:653-665.
13. Newman AM, Liu CL, Green MR, Gentles AJ, Feng W, Xu Y, Hoang CD, Diehn M, Alizadeh AA. Robust enumeration of cell subsets from tissue expression profiles. Nat Methods. 2015; 12:453-457.
14. Jiang P, Gu S, Pan D, *et al*. Signatures of T cell dysfunction and exclusion predict cancer immunotherapy response. Nat Med. 2018; 24:1550-1558.
15. Mariathasan S, Turley SJ, Nickles D, *et al.* TGFbeta attenuates tumour response to PD-L1 blockade by contributing to exclusion of T cells. Nature. 2018; 554:544-548.
16. Salmena L, Poliseno L, Tay Y, Kats L, Pandolfi Pier P. A ceRNA hypothesis: The rosetta stone of a hidden RNA language? Cell. 2011; 146:353-358.
17. Song X, Xie Y, Kang R, Hou W, Sun X, Epperly MW, Greenberger JS, Tang D. FANCD2 protects against bone marrow injury from ferroptosis. Biochem Biophys Res Commun. 2016; 480:443-449.
18. Cao F, Luo A, Yang C. G6PD inhibits ferroptosis in hepatocellular carcinoma by targeting cytochrome P450 oxidoreductase. Cell Signal. 2021; 87:110098.
19. Wu J, Wang Y, Jiang R, Xue R, Yin X, Wu M, Meng Q. Ferroptosis in liver disease: New insights into disease mechanisms. Cell Death Discov. 2021; 7:276.
20. Liu W, Zheng L, Zhang R, Hou P, Wang J, Wu L, Li J. Circ-ZEB1 promotes PIK3CA expression by silencing miR-199a-3p and affects the proliferation and apoptosis of hepatocellular carcinoma. Mol Cancer. 2022; 21:72.
21. Liu P, Xia P, Fu Q, Liu C, Luo Q, Cheng L, Yu P, Qin T, Zhang H. miR-199a-5p inhibits the proliferation of hepatocellular carcinoma cells by regulating CDC25A to induce cell cycle arrest. Biochem Biophys Res Commun. 2021; 571:96-103.
22. Li Z, Zhou Y, Zhang L, Jia K, Wang S, Wang M, Li N, Yu Y, Cao X, Hou J. microRNA-199a-3p inhibits hepatic apoptosis and hepatocarcinogenesis by targeting PDCD4. Oncogenesis. 2020; 9:95.

23. Li L, Wang H, Zhang J, Chen X, Zhang Z, Li Q. Effect of endothelial progenitor cell-derived extracellular vesicles on endothelial cell ferroptosis and atherosclerotic vascular endothelial injury. Cell Death Discovery. 2021; 7:235.
24. Zhang GY, Gao Y, Guo XY, Wang GH, Guo CX. MiR-199a-5p promotes ferroptosis-induced cardiomyocyte death responding to oxygen-glucose deprivation/reperfusion injury *via* inhibiting Akt/eNOS signaling pathway. The Kaohsiung J Med Sci. 2022; 38:1093-1102.
25. Brissot P, Ropert M, Le Lan C, Loreal O. Non-transferrin bound iron: A key role in iron overload and iron toxicity. Biochim Biophys Acta. 2012; 1820:403-410.
26. Casini A, Leone S, Vaccaro R, Vivacqua G, Ceci L, Pannarale L, Franchitto A, Onori P, Gaudio E, Mancinelli R. The emerging role of ferroptosis in liver cancers. Life (Basel). 2022; 12:2128.
27. Huang Y, Wang S, Ke A, Guo K. Ferroptosis and its interaction with tumor immune microenvironment in liver cancer. Biochim Biophys Acta Rev Cancer. 2022; 1878:188848.

Received June 1, 2023; Revised August 3, 2023; Accepted August 12, 2023.

[§]These authors contributed equally to this work.
**Address correspondence to:*
Chang Zhou, or Jianlin Zhou, College of Life Science, Hunan Normal University, 36 Lushan Road, Changsha, 410081, Hunan, China.
E-mail: zhouc@hunnu.edu.cn (Zhou C), jlzhou@hunnu.edu.cn (Zhou J)

Released online in J-STAGE as advance publication August 19, 2023.